

Developing an Ionospheric Scintillation



A team of researchers describes the development of a custom system for monitoring and collecting data on ionospheric scintillation and reports on its performance at facilities in the equatorial and arctic regions.

JAMES T. CURRAN, MICHELE BAVARO, AND JOAQUIM FORTUNY

EUROPEAN COMMISSION, JOINT RESEARCH CENTER, INSTITUTE FOR THE PROTECTION AND SECURITY OF THE CITIZEN, ISPRA (VA), ITALY

AIDEN MORRISON

SINTEF INFORMATION AND COMMUNICATION TECHNOLOGY DEPARTMENT, TRONDHEIM, NORWAY

Severe signal amplitude and phase scintillation induced by ionospheric activity can pose significant challenges to most commercial receivers and can degrade ranging accuracy, cause carrier-phase cycle slips, and even induce loss of lock on some satellites. The difficulties that receivers experience in tracking GNSS signals during such ionospheric activity directly translate to a difficulty in measuring this same activity.

Ionospheric scintillation typically has adverse effects at the synchronization and tracking stage of a GNSS receiver and, therefore, is a threat to all navigation receivers incorporating GNSS technology, including stand-alone, differential, assisted, and inertial-coupled receivers. As such, monitoring the ionosphere via GNSS signals is an important task, both to understand space weather and the atmosphere and to understand its effects on GNSS receiver operation and performance.

GNSS-based studies of the ionosphere are typically conducted using precision navigation receivers that track both the carrier and code phase, either on a satellite-by-satellite basis or collectively by means of a vector struc-

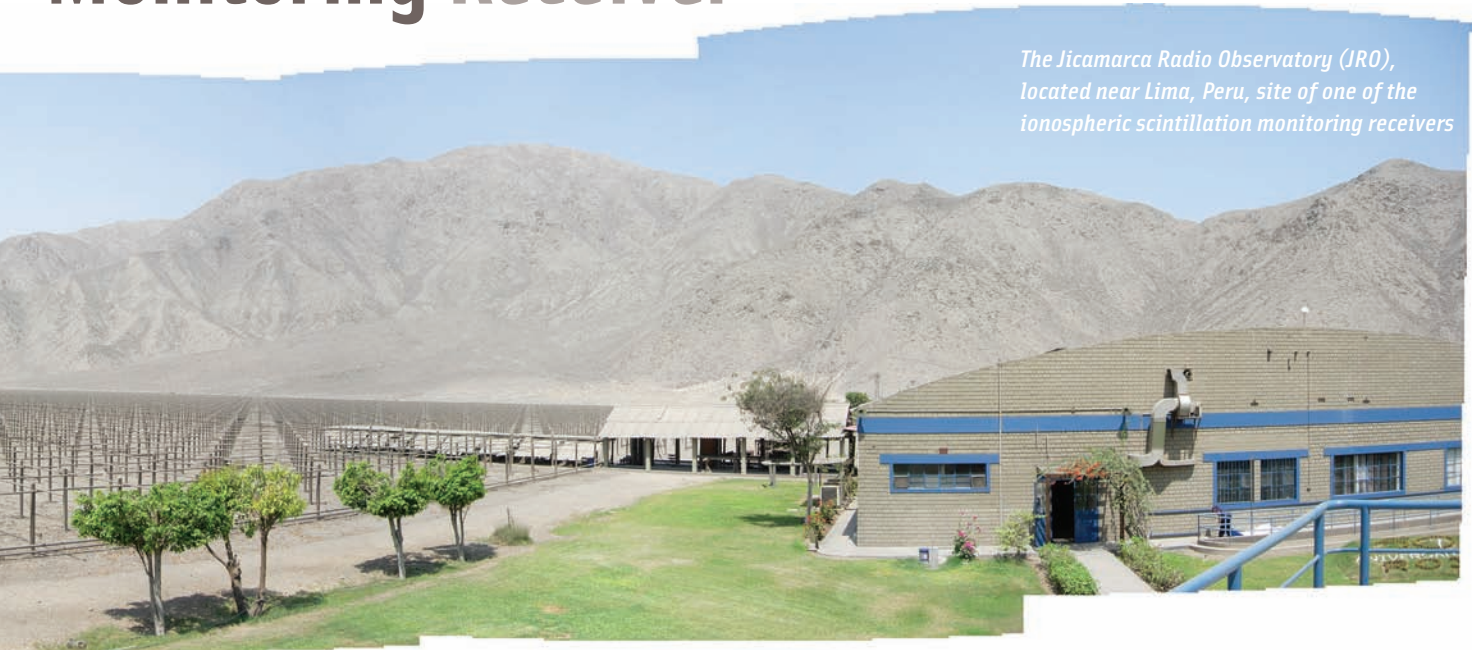
ture. Information relating to phase and amplitude scintillation is gathered from the receiver's estimate of the carrier phase and the receiver correlators values, respectively. The quality of these parameters, however, is directly influenced by how well the receiver can track the GNSS signals.

Under scintillation conditions these measurements are corrupted and degraded as the errors in the code and carrier tracking loops grow. Code-phase biases will manifest themselves as amplitude fades and carrier phase cycle-slips will appear as large, sudden phase fluctuations. Given such corrupted data, it can be difficult to distinguish between receiver-induced artifacts and ionosphere anomalies. Moreover, if a receiver cannot acquire or track the signal, these measurements are simply not available.

To tackle this problem, some receiver companies have produced variations of their precision receivers and post-processing software, which have been specifically configured and tuned to increase robustness under high ionospheric activity. These improvements are primarily in the area of baseband configuration, such as phase-lock loop

Monitoring Receiver

The Jicamarca Radio Observatory (JRO), located near Lima, Peru, site of one of the ionospheric scintillation monitoring receivers



(PLL) tuning, and in the area of measurement processing, such as identifying and rejecting scintillation-corrupted measurements, while the receiver architecture, in general, is similar to that of a typical high-precision navigation receiver.

Rather than pursue the route of tuning and calibrating a traditional receiver architecture, this article explores the custom design of a scintillation-monitoring receiver (SMR). The navigation capabilities of a traditional SMR are often redundant as such receivers are typically fixed at known coordinates.

Indeed the entire acquisition and tracking process is avoidable.

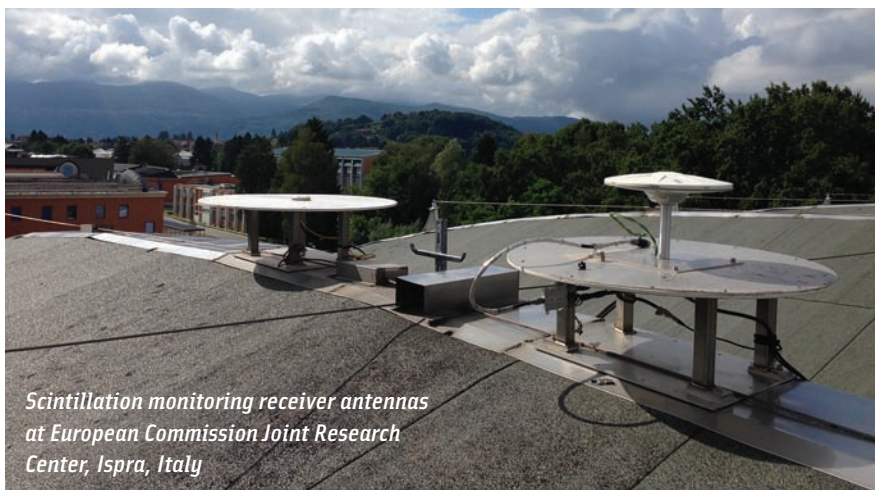
This latter fact is exploited in an SMR design that adopts an open-loop architecture. Instead of tracking the range and range-rate to each satellite in view, this architecture leverages knowledge of both the receiver and satellites positions in time and space to demodulate the received signals. In an inversion of the traditional navigation receiver, which uses measurements of signal parameters to compute an estimate of position and time, this open-loop architecture uses knowledge of position and time to esti-

mate local-replica signal parameters for demodulation purposes and does so in a purely feed-forward fashion.

Essentially an open-loop vector demodulation scheme, this approach reliably produces a series of baseband correlator values from which the deterministic phase process induced by satellite-to-user dynamics and receiver clock effects have been removed. This results in a series of complex correlator values modulated only by the amplitude and phase processes corresponding to the ionospheric activity. These values can then be processed to extract the phase and amplitude processes and produce traditional metrics such as phase scintillation index (σ_ϕ), the amplitude scintillation index (S4), or a variety of other scintillation characterizations.

Measuring Ionospheric Scintillation

Typically, the GNSS signal received at the antenna of a ground-based receiver is modeled as an ensemble of signals from each of the satellites in view, plus a thermal noise factor. Modern GNSS receivers employ either one or more heterodyne stages followed by sampling and digitization, or direct digital down-



Scintillation monitoring receiver antennas at European Commission Joint Research Center, Ispra, Italy

conversion to either a low or zero intermediate frequency (IF).

In either case, the result is a sequence of digitized samples, rendered at a rate of $1/T_s$, and can be approximated by:

$$r[k] = \sum_{i \in \text{Sig}} s_i(kT_s) + n(kT_s) \quad (1)$$

$$s_i(t) = \sqrt{2P_i(t)} d_i(t - \tau_i(t)) c_i(t - \tau_i(t)) \sin(\omega_i t + \theta_i(t)),$$

where S is the set of satellite signals in view, $s_i(t)$ denotes the i th signal received from the visible satellites, and $n(t)$ denotes the additive thermal noise.

The various parameters in (1) represent the following signal properties: P_i is the total received signal power in watts; ω_i is the nominal IF carrier frequency in units of rads^{-1} ; $d_i(t)$ represents the bi-podal data signal, if present; $c_i(t)$ represents the combination of the secondary code, the primary spreading sequence and the sub-carrier; $\theta_i(t)$ is the total received phase process including propagation delays, satellite-to-user dynamics, atmospheric effects, and satellite clock effects; the process $\tau_i(t)$ represents the total delay observed at the receiver, including propagation delay, satellite clock effects and atmospheric delays.

The carrier phase term, $\theta_i(t)$ in (1) represents a number of distinct phase processes and can be represented as the following linear combination:

$$\theta_i(t) = \theta_0 + \theta_{\text{LOS}}(t) + \theta_{\text{SV Clk.}}(t) + \theta_{\text{Rx Clk.}}(t) + \theta_{\text{Atm.}}(t), \quad (2)$$

where θ_0 represents some arbitrary initial phase, $\theta_{\text{LOS}}(t)$ represents the phase process induced by the line-of-sight geometry and dynamics between the satellite and the receiver, $\theta_{\text{SV Clk.}}(t)$ and $\theta_{\text{Rx Clk.}}(t)$ respectively represent the phase processes induced by errors in the satellite and receiver clocks, and $\theta_{\text{Atm.}}(t)$ represents the phase process induced by the atmosphere through which the signal propagates.

Similarly, we can represent the received power, $P_i(t)$ in (1) by the product:

$$P_i(t) = P_{\text{SV}} \times L_{\text{LOS}}(t) \times L_{\text{Atm.}}(t) \times L_{\text{Rx}}(t), \quad (3)$$

where P_{SV} represents a nominal transmitted power, $L_{\text{LOS}}(t)$ represents free-space loss across the line-of-sight range the satellite and the receiver, $L_{\text{Atm.}}(t)$ represents the effective power loss induced by the atmosphere through which the signal propagates, and $L_{\text{Rx}}(t)$ represents the loss (or gain) induced by the receiver antenna, front-end, and digitization process. The terms $\theta_{\text{Atm.}}(t)$ and $L_{\text{Atm.}}(t)$ are of interest here.

As GNSS signals are received at the Earth at a very low nominal power, typically below the thermal noise floor, receivers need to employ a digital matched filter (DMF) to help despread the signals, introducing sufficient correlation-gain (of the order of 30 to 40 decibels) to enable a receiver to acquire and track the signals. The DMF operation can be expressed as follows:

$$Y_i[n] = \frac{1}{T_I} \sum_{k=n \frac{T_I}{T_s}}^{(n+1) \frac{T_I}{T_s} - 1} \left(r(kT_s) c_i(kT_s - \hat{\tau}_i(kT_s)) e^{-j(\omega_i(kT_s) + \hat{\theta}_i(kT_s))} \right), \quad (4)$$

where the \hat{a} denotes the receivers estimate of parameter a, and the term $Y_i[n]$ is known as the correlator value and is computed across an interval T_I , which typically ranges from one to one

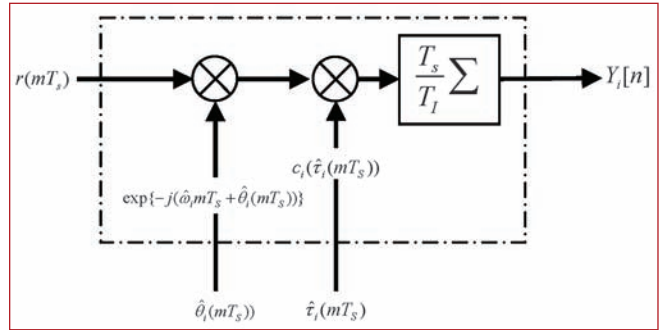


FIGURE 1 Block diagram of a digital matched filter

hundred milliseconds. **Figure 1** presents a block diagram of this operation.

A typical GNSS receiver produces one or more correlator values, with prescribed code and frequency offsets relative to the current estimates of τ_i and θ_i . For example a standard delay-lock loop (DLL) will require two additional correlator values, generated with “early” and “late” code replicas. In any case, the receiver will process the correlator values by employing either a set of code and carrier tracking loops or a so-called central vector-tracking loop, to recursively estimate the next set of values of τ_i and θ_i .

Although both the code and carrier phases are representative of the range and range change between the satellite and the receiver, they are generally used in different applications due to their significantly different periods. As current GNSS signals have wavelengths in the range of 18 to 27 centimeters, carrier phase measurements can provide a particularly sensitive means of observing changes in the propagation delay. For the purposes of atmospheric scintillation monitoring, when only the temporal or spatial variations in the signal delay are of interest, the carrier phase is generally utilized.

Signal Power as a Scintillation Metric

Traditionally, researchers have examined the effects of ionospheric scintillation on the received signal amplitude and phase using statistics known as the amplitude and phase scintillation indices, respectively denoted S_4 and σ_ϕ . Essentially, S_4 is a measure of the variation of instantaneous received signal amplitude relative to the average received signal amplitude over a certain period of time, and σ_ϕ is a measure of the variations in received signal phase relative to the nominal phase trajectory that would be observed under non-scintillation conditions.

In both cases, the temporal variations are examined relative to a non-constant value, which is not directly accessible to the receiver; consequently, care must be taken when performing these measurements. In the case of S_4 , this non-constant value is the nominal received signal power, and in the case of σ_ϕ it is the nominal phase trajectory.

In general, receivers implement a so-called de-trending operation that endeavors to separate the deterministic, slowly varying contributions to the amplitude and phase processes, $P_i(t)$ and $\theta_i(t)$ — induced, for example, by line-of-sight displacement, the receiver antenna, and the local oscillator — from the stochastic, more rapidly varying scintillation-related contri-

butions. Historically, receiver designers have exploited the spectral separation of the deterministic “trends” and the random scintillation effects using high- and low-pass filters for this purpose.

As carrier phase is regularly employed for navigation purposes, an estimate of the integrated Doppler (θ) is readily available in many GNSS receivers, in particular those designed for high-precision applications. Although GNSS receivers regularly use the received signal power or carrier-to-noise ratio (C/N_0) as an indicator of signal quality, they do not routinely provide a direct measure of the instantaneous received signal power. Estimates of C/N_0 that are provided may be heavily smoothed and are often provided at a relatively coarse resolution. Thus, receivers intended for scintillation monitoring often provide direct access to the “prompt” correlator values or provide a dedicated signal power measurement.

When computing a measure of the instantaneous signal power, care must be taken to ensure that the receiver’s automatic gain control (AGC) circuit has been disabled, or that variations in gain are accounted for. As the power estimate is later normalized, any estimate of the received power, which is linearly proportional to the received power across the expected received power range, will suffice.

This estimate of signal power is often termed *signal intensity* and is denoted here by I . In many cases this is calculated by means of additional intermediate variables representing signal power or, alternatively, can be calculated directly from the correlator values, Y_i .

In the work described in this article, an instantaneous measure of the signal power is computed as the square magnitude of the complex correlator values, minus an estimate of the thermal noise contribution, thus:

$$\hat{P} = |Y_i|^2 - 2\sigma^2 \quad (5)$$

When scintillation monitoring has been conducted using low Earth orbit (LEO) satellites that have orbital periods between one and two hours, such as the U.S. Air Force’s Wideband (P76-5) project in the 1970s, the received signal

power exhibits a deterministic trend that changes quite rapidly. To compensate for this effect, a de-trending operation is commonly applied to remove the variation in signal power, whereby the power estimate is divided by a low-pass version of itself. This technique often employs a sixth-order Butterworth low-pass filter with a 0.1-hertz bandwidth such that the signal intensity, I , is equal to the de-trended signal power measurement.

In contrast, when scintillation monitoring uses middle Earth orbit (MEO) GNSS signals, which emanate from satellites having orbital periods in the range of 11 to 14 hours, this signal power variation is not so apparent. As a result, a detrending operation is not necessarily required and is omitted by some scintillation monitoring receivers. In this case, a GNSS SMR calculates the S_4 metric from I as follows:

$$S_4 = \left(\langle I^2 \rangle_T - \langle I \rangle_T^2 \right) / \langle I \rangle_T^2 \quad (6)$$

where the notation $\langle \cdot \rangle_T$ denotes the temporal average over some fixed period, T . Various values of T have been employed in the literature with the more widely accepted values being 20 and 60 seconds.

Although we can ignore the signal power variations of some MEO satellite signals, the deterministic trend of the carrier phase is still significant and must be removed. Moreover, as indicated in (2), the observed carrier phase has a number of non-orbit-induced contributions. A standard GNSS receiver typically derives carrier phase observations via a closed loop phase-tracking algorithm, such as a PLL, which will produce the entire phase trajectory, including the Doppler-induced phase trend, receiver and satellite oscillator effects, and the ionospheric contribution.

The method of σ_ϕ calculation implemented in such a receiver typically involves three steps. First, the phase of the received GNSS signal is reconstructed and sampled at a fixed sample rate, typically 50 hertz. Second, in order to extract the

scintillation part of the phase process, the phase is de-trended using a sixth-order Butterworth high-pass filter having 0.1-hertz bandwidth. The result is a zero-mean stochastic phase, denoted here by ϕ , which, ideally, contains only the scintillation-related phase. Finally, the variance of the de-trended phase process is calculated over fixed-length, non-overlapping periods of T seconds, via:

$$\sigma_\phi = \langle \phi^2 \rangle_T - \langle \phi \rangle_T^2, \quad (7)$$

Figure 2 presents a simplified block diagram depicting the calculation of these two scintillation indices from the raw receiver measurements.

A Custom Scintillation Monitoring Receiver

In the design of a custom SMR, we took specific care to identify the unique requirements of a monitoring receiver’s architecture, as distinct from that of a traditional navigation receiver. By shirking the duties of positioning and navigation and by relying on some external aiding information, we could relax some design requirements. Conversely, by adopting a feed-forward demodulation scheme, other requirements became more stringent.

Figure 3 presents a simplified block diagram of the complete receiver, comprised of three distinct sub-systems: a data-acquisition section, an open-loop demodulation unit, and a unit that implements the atmosphere monitoring algorithms.

Data Acquisition. In essence, the data acquisition (DAQ) portion of the SMR receiver is implemented as any typical GNSS front-end, incorporating an antenna, a reference clock, down-converters, and digitizers that produce streams of digitized IF samples.

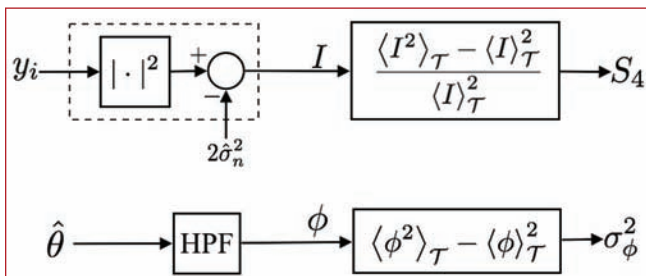


FIGURE 2 Calculation of scintillation indices from receiver variables

Being a dispersive medium, the ionosphere has a significantly different impact on signals transmitted at different carrier frequencies. For the purposes of scintillation monitoring, therefore, observing as many different frequencies as possible by capturing data in multiple bands may produce interesting results. The number of bands that can be observed is ultimately limited by the throughput and storage capabilities of the receiver and host computer; therefore, design criteria such as sampling rate and digitizer resolution must be carefully considered.

With the intention of observing GNSS signals under line-of-sight and interference-free conditions, an SMR can use a low quantizer resolution, either one- or two-bit, without incurring any significant loss in signal quality. Moreover, as the system is not required to perform any ranging functions, the received GNSS signals can be significantly band-limited. Accordingly, because the shape and sharpness of the ranging code correlation function is not of interest for an SMR, band limiting manifests itself only as a loss in received signal power.

Gain and timing requirements imposed by the SMR's open-loop architecture are key factors for consideration. Each sample captured by the digitizer must be associated with a precise receive time, which is used by the demodulator in the generation of local replica signals. This time is sourced from the reference clock and, ideally, will coincide with the true GNSS time.

Examining (2) and (4), we can see that the reference clock phase noise will contribute to the observed phase scintillation measurement. Also, errors in the reference clock will manifest themselves in misalignments between the received spreading code sequence and local replica, as seen in (4), thereby inducing variations in the magnitude of Y_i . To minimize these effects, the reference clock should offer good short- and long-term stability. Moreover, the clock should exhibit a very low phase noise, and the bias and drift terms should either be negligible or accurately modeled.

The behavior of the AGC has a direct influence on the observed variations in the signal power at IF that, as can be seen by inspection of (3) and (4), can cor-

rupt measurements of S_4 . To avoid this, the AGC must be configured to either maintain a constant gain over the observation period or exhibit a sufficiently low slew-rate so as to allow its effect to be removed via de-trending. Alternatively, the AGC gain may be recorded to facilitate post-correlation normalization. In the present design, we conducted a one-time calibration of the AGC to choose a fixed gain.

Open-Loop Receiver Architecture. The signal demodulator is the heart of the receiver architecture, processing the time-tagged IF samples captured by the DAQ to produce baseband correlator values. Unlike a traditional GNSS receiver, the SMR demodulator does not rely on feedback mechanisms to produce estimates of the current signal parameters such as carrier and code phase. Rather, it relies on prior knowledge of the satellite and user trajectories, time, and some broadcast propagation models. As such, it performs the demodulation in an open-loop manner, as depicted in Figure 4.

In this study, the monitoring receiver has been installed at a well-surveyed, fixed location, such that the position of the antenna phase center is known to centimeter accuracy. Knowledge of the satellite position can be derived either through broadcast or precise ephemerides. If post-processing data that has been collected and stored some time previously, then collated broadcast ephemerides can be sourced from sources such as the International GNSS Service.

Alternatively, for live processing, ephemerides can be sourced from nearby reference stations. One particular benefit of this scheme is that signals can be readily tracked even if they are well below the data-demodulation threshold. Provided that one station, somewhere on Earth, has successfully extracted a valid ephemeris record, the received satellite signal can be processed. As ionospheric activity can be quite spatially uncorrelated, one station may enjoy perfect conditions for receiving signals while another, some hundreds of kilometers away, may observe severe scintillation.

Each sample stream originating from the DAQ has an associated cen-

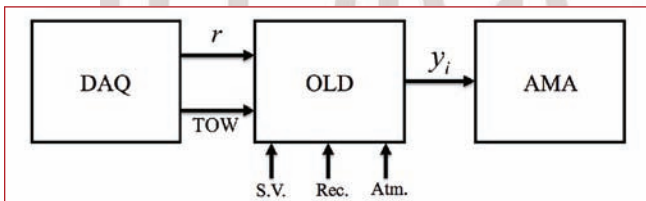


FIGURE 3 Block diagram of the open-loop receiver

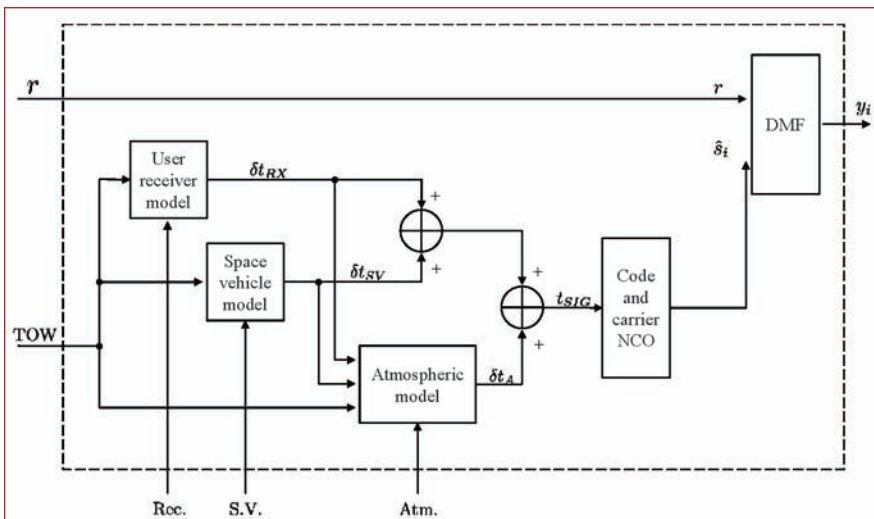


FIGURE 4 Open-loop demodulation scheme

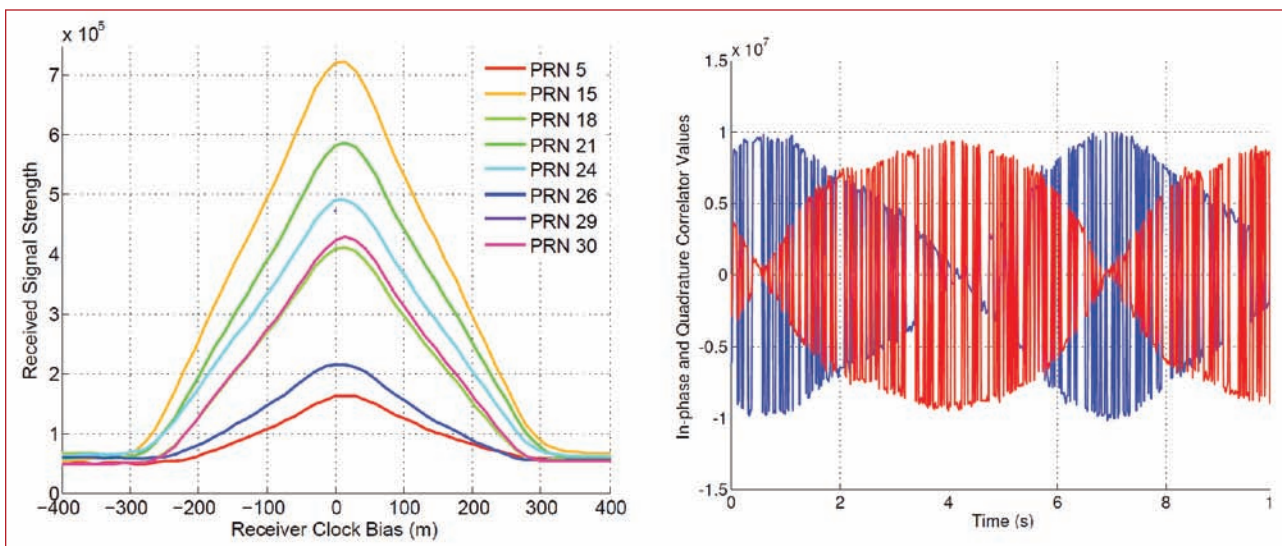


FIGURE 5 Open-loop demodulation of GPS L1 C/A signals

ter frequency and bandwidth, and each sample within that stream has an associated time-tag. For each of the satellite signals that lie within the sample stream bandwidth, a visibility check is computed using the corresponding ephemeris record and the sample time-tag. The visibility check coarsely evaluates the elevation from the known receiver position to the satellite position, computed at the current receiver time, and compares it to an elevation mask.

For each satellite signal that is deemed visible, the host computer calculates, via recursion, the effective transmit-time, incorporating known receiver biases. A sample of the local replica signal is then generated to correspond to this transmit time, including carrier, subcarrier, and primary (and secondary) code, and used to demodulate the received sample. As the effective transmit time is computed directly, the demodulated signal can be accumulated, or integrated, and dumped at boundaries of the transmit time, in this case at 20-millisecond epochs of the transmit time.

The left panel of **Figure 5** shows an example of the average complex envelope of the correlator values versus receiver clock bias for a selection of GPS L1 C/A signals. As can be seen, the envelope exhibits the classical cross-correlation function observed during a traditional acquisition process. Evident also is the fact that the demodulation process can only align the local replica signals with

their received counterparts to a degree commensurate with the accuracy of the local clock, the satellite ephemeris, the atmospheric model (troposphere and ionosphere group delay), and various receiver delays and biases.

Despite these biases, the “aligned” or “prompt” correlator can be readily placed sufficiently close to the true delay so as to capture the majority of the received signal power, thus being sufficiently aligned for the purposes of scintillation monitoring. The right-hand panel of **Figure 5** shows a time-series of this prompt correlator wherein the residual errors after the open-loop demodulation can be seen as a rotation of the complex correlator values over time.

Design Criteria & Expected Performance. As mentioned previously, the scintillation monitoring receiver is not required to perform any ranging functions and, therefore, is not sensitive to band-limiting of the received GNSS signals. Indeed, reduction in the received signal bandwidth is only manifest as a reduction in the received C/N_0 .

Similarly, as the receiver is not expected to encounter any interference or jamming, it is not particularly sensitive to front-end digitization. Thus, even for one-bit digitization, it will experience only a modest reduction in the received C/N_0 . Therefore, in the interest of reducing data-throughput and storage requirements, both the receiver

bandwidth and digitizer resolution are reduced as far as can be tolerated.

To identify the maximum C/N_0 loss that can be endured, its effect on the final scintillation measurements must be examined. Indeed, the influence of signal C/N_0 on the quality of scintillation indices poses an interesting problem in its own right, aside from its application to loss budgeting, and bears examining to determine how the accuracy and meaningfulness of metrics such as S_4 and σ_ϕ degrades with reduced C/N_0 .

In particular, it is worth understanding if a threshold exists below which scintillation indices should not be extracted from a received signal. We can address this question by studying the behavior of these metrics in the absence of scintillation, across a range of received C/N_0 conditions. In this way, we can assess the thermal-noise contribution to each of these scintillation measurements and decide when it is too large or is likely to dominate real scintillation contributions. Moreover, having quantified the thermal noise factor, we may in fact be able to compensate for its effect by removing this bias.

If we model the correlator values, Y_r , as non-zero mean Gaussian random variables, with mean and variance dictated by the received C/N_0 , then the thermal noise contributions to both the amplitude and phase scintillation indices can be modeled as

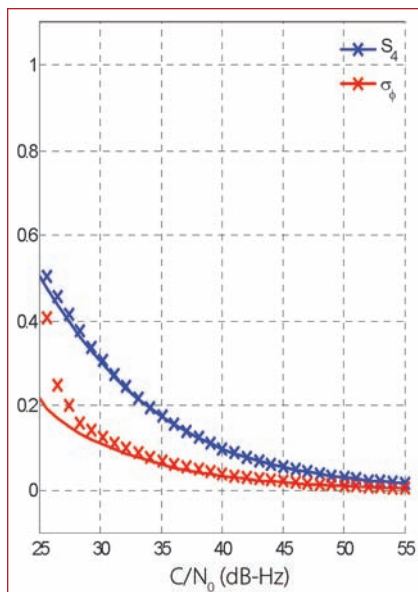


FIGURE 6 Thermal noise contribution to the measured S_4 and σ_ϕ scintillation indices versus received carrier-to-noise-floor ratio. Solid lines represent the predicted value, as per equations (8), while the markers represent simulation measurements.

$$\sigma_n^2 = \frac{C/N_0}{2T_I} \tag{8}$$

$$\sigma_\phi^{\text{Therm}} = \frac{\sigma_n}{\sqrt{2}}$$

$$S_4^{\text{Therm}} = \frac{\sqrt{4(\sigma_n^4 + \sigma_n^2)}}{1 + 2\sigma_n^2}$$

Figure 6 depicts a comparison of the expressions in (8) and simulated measurements, showing good agreement for high to moderately low C/N_0 values. One useful application of these results is the assessment of the increase in the thermal noise contribution to the scintillation indices that would be observed for a given loss in C/N_0 .

The rate of increase of the thermal noise contribution to the scintillation indices with reducing C/N_0 is relatively low for signals received in the range of 40 to 50 dB-Hz. For example, signals received between 45 and 50 dB-Hz would experience a negligible (<0.05) thermal noise contribution to the amplitude scintillation index. Thus, if a processing loss of, for example, three to five decibels were incurred on such signals as a result of band-limiting and digitization, the measured scintillation indices would remain relatively unchanged.

This is not the case, however, for weaker signals having a C/N_0 below, for example, 40 dB-Hz, which experience a much more significant thermal noise contribution to the scintillation indices. In such cases the scintillation indices may simply be unreliable or, alternatively, they may need to be corrected so as to remove the thermal noise bias, using equations (8).

In light of these figures, a modest amount of receiver-based processing losses can clearly be tolerated without inducing any discernible degradation in scintillation monitoring performance. Given a wealth of literature on the topic of receiver-based processing losses, we can determine a suitable trade-off between implementation cost and complexity and C/N_0 loss.

This is noticeably different from applications such as a high-precision navigation, where a far more direct relationship exists between signal quality and measurement quality. This work explores the use of one- and two-bit digitization and capturing only the main lobe(s) of the GNSS signals.

Design and Receiver Implementation

A software-defined-radio approach requires a data acquisition unit, which performs appropriate analog signal conditioning (filtering, amplification, frequency translation), digitizes, and transfers the digital data to a host processing unit to performing the signal processing.

At the Joint Research Center in Ispra, researchers have developed a four-channel data collection unit dubbed “Fourtune” to perform the task. Each of the four RF channels is capable of tuning to any GNSS frequency and digitize it to complex eight-bit samples having a bandwidth up to 60 megahertz. A field programmable gate array (FPGA) in the data path performs medium-complexity signal processing such as decimation, digital filtering, quantization, channel combination, buffering and data packing. A USB microcontroller defines the behavior of all other elements on the board, setting the channels’ center frequency, the ADC sampling frequency,

the FPGA firmware, and the ADC timing characteristics.

One limitation of the current version of the DAQ unit is the throughput of the USB 2.0 standard, which has been demonstrated to be stable only up to 30 MBps. A revision of Fourtune currently in production employs USB 3.0, which also extends the number of channels from four to eight. Figure 7 improved Fourtune design and its final implementation, including external disciplined oscillator is shown in Figure 8.

One important feature of the board is the clocking path, which is finely tuned for simultaneous sampling at all ADCs. It specifically enables the operation of multiple boards from a common reference, via the use of zero-delay buffers. An on-board inter-integrated circuit (I²C) digital-to-analog converter (DAC) allows for fine-tuning the frequency of the onboard voltage-controlled oscillator. As the I²C bus is exposed on a four-pin header, the configuration software can also control external I²C peripherals and, in particular, external voltage-controlled clock references as described later in this article.

In fact, a particularly stringent requirement of the proposed signal-processing scheme is for a reference clock that is precise and stable, both in terms of deterministic long-term drift and stochastic, short-term phase stability. Although the scheme has been initially validated using state-of-the-art atomic reference oscillators, the present work demonstrated an alternative solution, which employs the periodic disciplining of an otherwise free-running ovenized crystal oscillator.

This solution implements a modeling and disciplining scheme for a voltage-controlled, ovenized crystal oscillator (VC-OCXO), using software-side modeling and compensation for residual clock errors. The refurbished oscillator used exhibits low phase noise and good long-term, or holdover, performance. The output of the clock is a seven dBm sine wave, which is both buffered for direct use and also converted to CMOS for devices requiring a digital reference.

The Fourtune front-end can be reconfigured in software, which allows

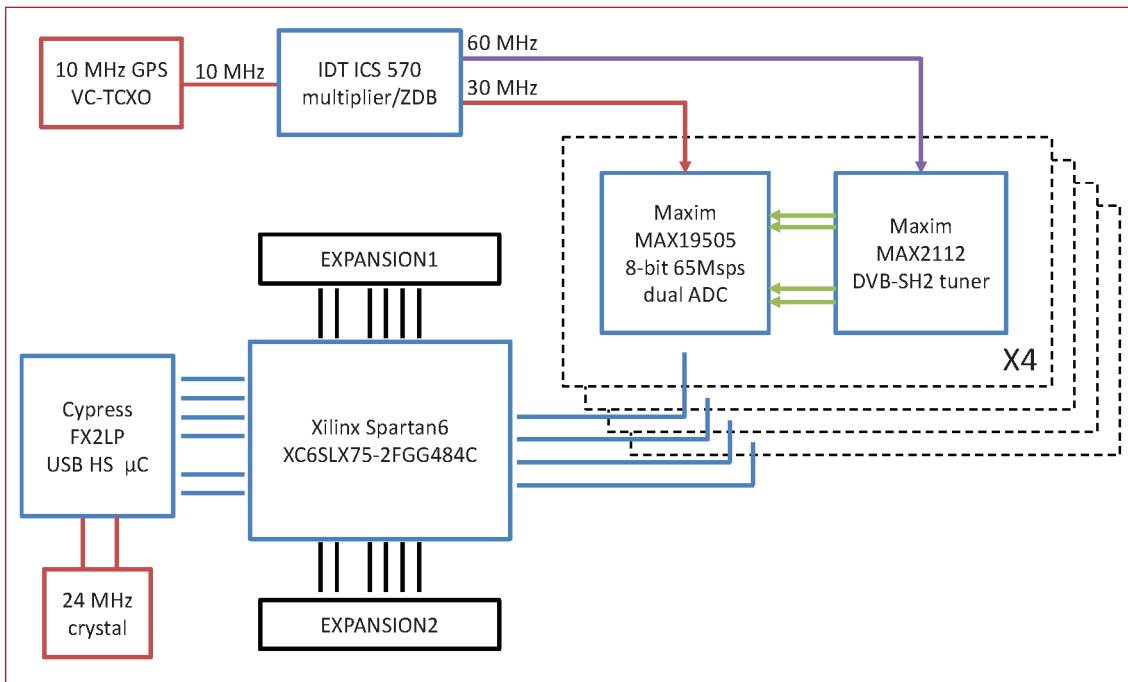


FIGURE 7 Fourtune architecture block diagram

for some degree of flexibility. Some of the possible configurations include:

- Galileo E1 and E6 at 15-megahertz bandwidth (2-bit complex), plus Galileo E5 at 60-megahertz bandwidth (1-bit complex). This configuration covers all Galileo signals.
- Galileo E1, GPS L2, Galileo E6, GPS L5 — all at 15-megahertz bandwidth (2-bit complex). This configuration covers triple-frequency GPS and Galileo.
- L1 at 60-megahertz bandwidth (1-bit complex) and L2 at 30-megahertz bandwidth (2-bit complex). This configuration covers all GPS and GLONASS satellites on two frequencies, guaranteeing maximum availability.

One of the caveats when using different bandwidths in the front-end channels is the need to calibrate the hardware delay introduced by the analog baseband filter, which increases as the filter becomes narrower. However such calibration is a one-time process, after which appropriate corrections for inter-channel biases can be applied post-mission.

An example spectrum and sample-histogram for a single, eight-megahertz channel tuned to L1, sampled as eight-bit complex samples at a rate of 15 Msps is

shown in **Figure 9**. Note the characteristic main-lobe of the aggregate GPS L1 C/A signals visible above the thermal noise floor.

The open-loop receiver has been implemented entirely in software as a portable, cross-platform executable. Written entirely in compliance with the ISO C++11 standard, it has been successfully compiled and run on various distributions of Linux, Mac, and Windows operating systems, on both 32-bit and 64-bit machines. This flexibility is necessary when running the receiver on a remote host machine, located at a scintillation-monitoring site.

To provide the most versatility, the SMR's software has been written to support multiple frequencies and systems and has little or no inherent assumptions about the kind of signals it processes. Internal variables are, where possible, floating point complex variables, averting any overflow issues that can arise when processing high-resolution IF datasets.

Once invoked, the receiver can automatically fetch and interpret RINEX 2.X and 3.X navigation files from any of a number of IGS repositories, will populate its processing channels with all satellite signals deemed visible, and begin to process the IF data. For reasons of

efficiency, a multi-threaded scheme has been adopted, specifically written to facilitate compiler/optimizer-level vectorization. Depending on the machine resources and the data-set sample rate, the receiver may support real-time or faster-than-real-time operation. Various optimizations of the code yield real-time operation when processing 10, or fewer, satellite signals on one IF stream sampled at five Msps or less.

The current configuration of the receiver produces 50-hertz observations for each signal of each satellite visible above an elevation mask of five degrees.



FIGURE 8 Fourtune front-end and GNSS-disciplined reference oscillator

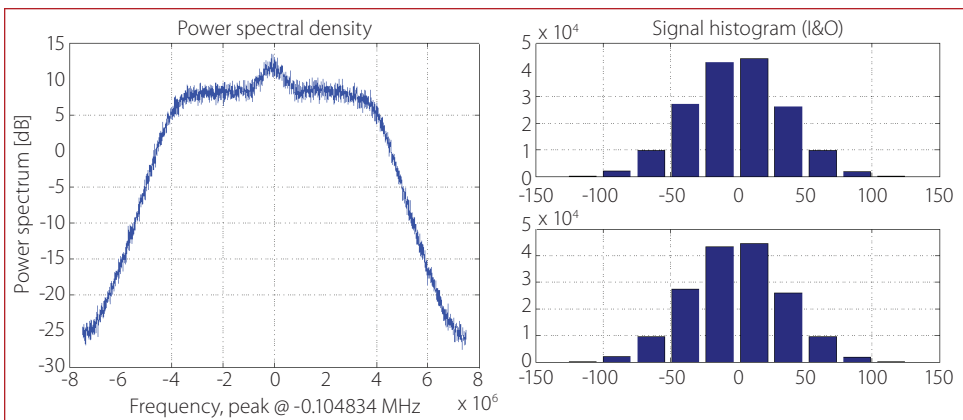


FIGURE 9 Example-spectrum and sample histogram for a single, eight-megahertz channel tuned to L1.

Observation data include transmit time, in-phase and quadrature correlator values, C/N_0 , signal intensity, S_4 , de-trended phase, and σ_ϕ . For the sake of data-storage, only the pilot component of composite signals, such as Galileo E1BC and GPS L2C, are processed.

Test Locations

The scintillation-monitoring receiver described here has been deployed in a number of locations where high ionospheric activity is expected, including one high-latitude and two equatorial stations, as illustrated in Figure 10. One is installed at the Jicamarca Radio Observatory (JRO), located near Lima, Peru, which has been online since April 2012; the second is at the Hanoi University of Science and Technology in Vietnam and has been online since February 2013; and the third is located at SINTEF in Trondheim, Norway and has been online since July 2014. The particular results presented in the following sections have been collected at the Hanoi station.

The Hanoi station SMR architecture was implemented using a collection of off-the-shelf components, as shown in Figure 11. This implementation uses a choke ring antenna connected to an universal software radio peripheral (USRP) front-end driven by a low phase noise rubidium clock. The host PC was connected to an array of hard-drives. The IF data streamed from the USRP was stored for post-processing, which allows software-only processing via the technique described here or replay directly to hardware-receivers for fur-

ther receiver-testing or data examination. We used a commercial atmospheric monitoring receiver as the reference unit for comparison.

The configuration is automated to capture a series of 20-minute, single-frequency IF recordings each day. The

USRP is configured to capture a five-megahertz band, centered at 1575.42 MHz as 16-bit, zero-IF data. These datasets are then physically transported to the laboratory for post-processing and categorized according to the severity of the observed scintillation. Also, select datasets are down-sampled, re-quantized and compressed to enable retrieval via file-transfer protocol (FTP) or shared cloud-storage.

The Information and Communication Technology (ICT) Department at the SINTEF campus in Trondheim Norway, maintains another SMR site. Located at 63.5 degrees north geographic latitude and geomagnetic latitude of approximately 62 degrees, this region is frequently traversed by the edge of the auroral oval,



FIGURE 10 Locations of data capture discussed in this study include two equatorial zone locations – Lima, Peru, and Hanoi, Vietnam – and one high-latitude location within the auroral zone at Trondheim, Norway. Also indicated is the location of the JRC GNSS Laboratory in Ispra, Italy.

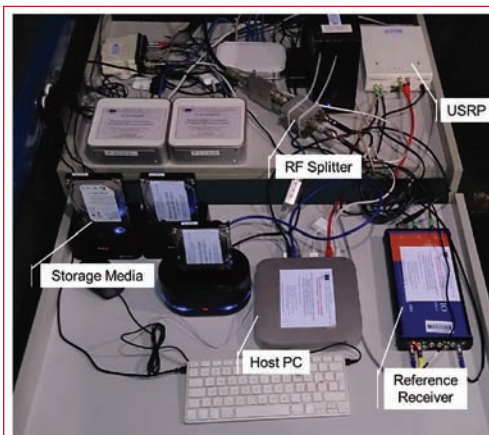
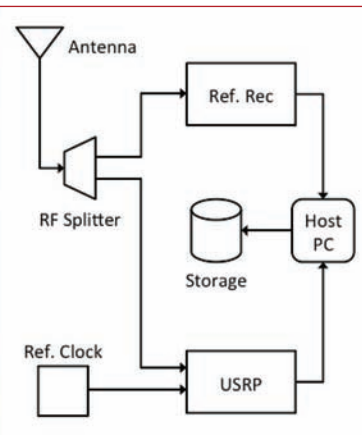


FIGURE 11 Experimental setup at the Jicamarca Radio Observatory, Lima, Peru



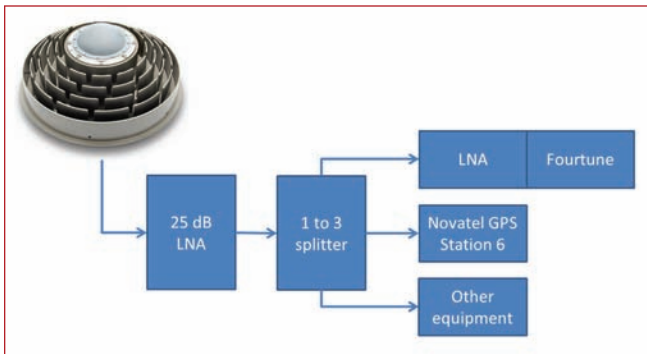


FIGURE 12 Equipment configuration at SINTEF, Norway.

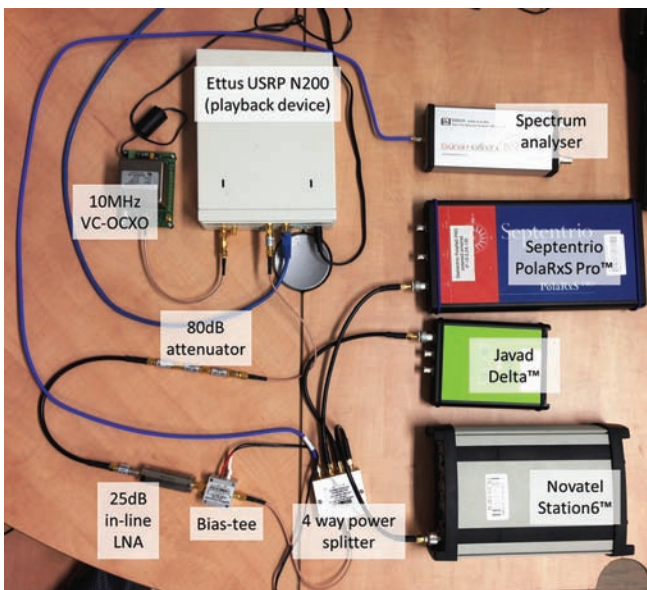


FIGURE 13 Playback equipment and test-bench configuration

an atmospheric region of charged particles centered over the geomagnetic North Pole, where phase scintillation is frequently observed.

The hardware configuration used at the SINTEF campus in support of this study included the use of a permanently installed triple band (B1/L1/E1/G1, L2/G2/B2/E6, L5/E5a/E5b/B3) choke-ring antenna, which fed the Fortune front-end as well as the other SINTEF GNSS receivers. **Figure 12** shows the antenna installation and signal distribution chain used at SINTEF ICT.

The antenna includes an internal 40-decibel low noise amplifier (LNA), but its installation point on the roof of the SINTEF ICT building requires the use of a long distribution cable that, in turn, necessitates an additional LNA prior to the splitter. After the splitter a final amplification stage is employed, acting as a fixed-value gain control to ensure near-optimal use of the available quantization levels.

Data collected at this site is processed remotely, using the open-loop scheme described in this article. The resulting scintillation indices are examined to determine whether or not the IF data should be reduced, compressed, and archived. These include datasets containing higher than usual ionospheric

activity, those corresponding to forecast geomagnetic storms, and those for which tracking difficulties were observed in the commercial receivers.

Benchmarking Against Commercial Receivers

Currently, ionospheric scintillation monitoring is conducted using commercial navigation receivers, mostly of the high-precision or survey type, observing multiple GNSS frequencies. In our research, we used an ionospheric monitoring and space weather receiver and an ionospheric scintillation and TEC (total electronic count) monitor receiver, as well as another GNSS receiver for reference. We collected datasets exhibiting both high and negligible ionospheric activity and processed them using both these GNSS receivers and the proposed open-loop receiver to demonstrate the equivalence of the traditional techniques and our new approach. Post-processing of the data includes a comparison of the traditional scintillation metrics, σ_ϕ and S4, between the commercial receivers and the new receiver architecture in terms of quality and availability.

We extracted the scintillation measurements from this collection of receivers by conductive re-broadcasting the recorded IF dataset using a radio peripheral playback device, as depicted in **Figure 13**. In order to ensure low clock drift and high phase stability, we used an ovenized crystal oscillator, which had been recently disciplined to the GPS time scale, as a reference for the playback device.

We took care to condition the playback signal appropriately so as to ensure that the signal arriving at the receivers under test was typical of normal operating conditions. Although the recorded IF dataset was broadcast at a bandwidth of only 5 megahertz, these receivers probably observe a bandwidth far greater than this — in the range of 40 to 100 megahertz. We therefore attenuated the broadcast signal to within 3 decibels of the ambient thermal noise floor, using 80-decibel inline attenuators.

Next, we amplified the combined signal and additive thermal noise using an inline LNA to a level that would be typical of the output of an active GNSS antenna. This signal was then split four ways and fed to each of the three receivers and a digital spectrum analyzer. We operated the receivers in the default, “out-of-the-box” configuration, with the exception that the clock-steering functionality was disabled for the ionospheric scintillation and TEC monitor receiver, as per its operating manual recommendations.

For each of the receivers, a custom script was written to configure the receiver and stream the raw measurements to the host computer. In the case of the ionospheric monitoring and space weather receiver, these raw measurements were post-processed using proprietary software from the receiver manufacturer to produce the series of scintillation indices. In the case of the ionospheric scintillation and TEC monitor receiver, the scintillation indices were included as part of the raw measurements recorded from the receiver.

In contrast, not being a dedicated space-weather receiver, the reference GNSS survey receiver did not natively provide scintillation indices. It did, however, provide access to high-rate

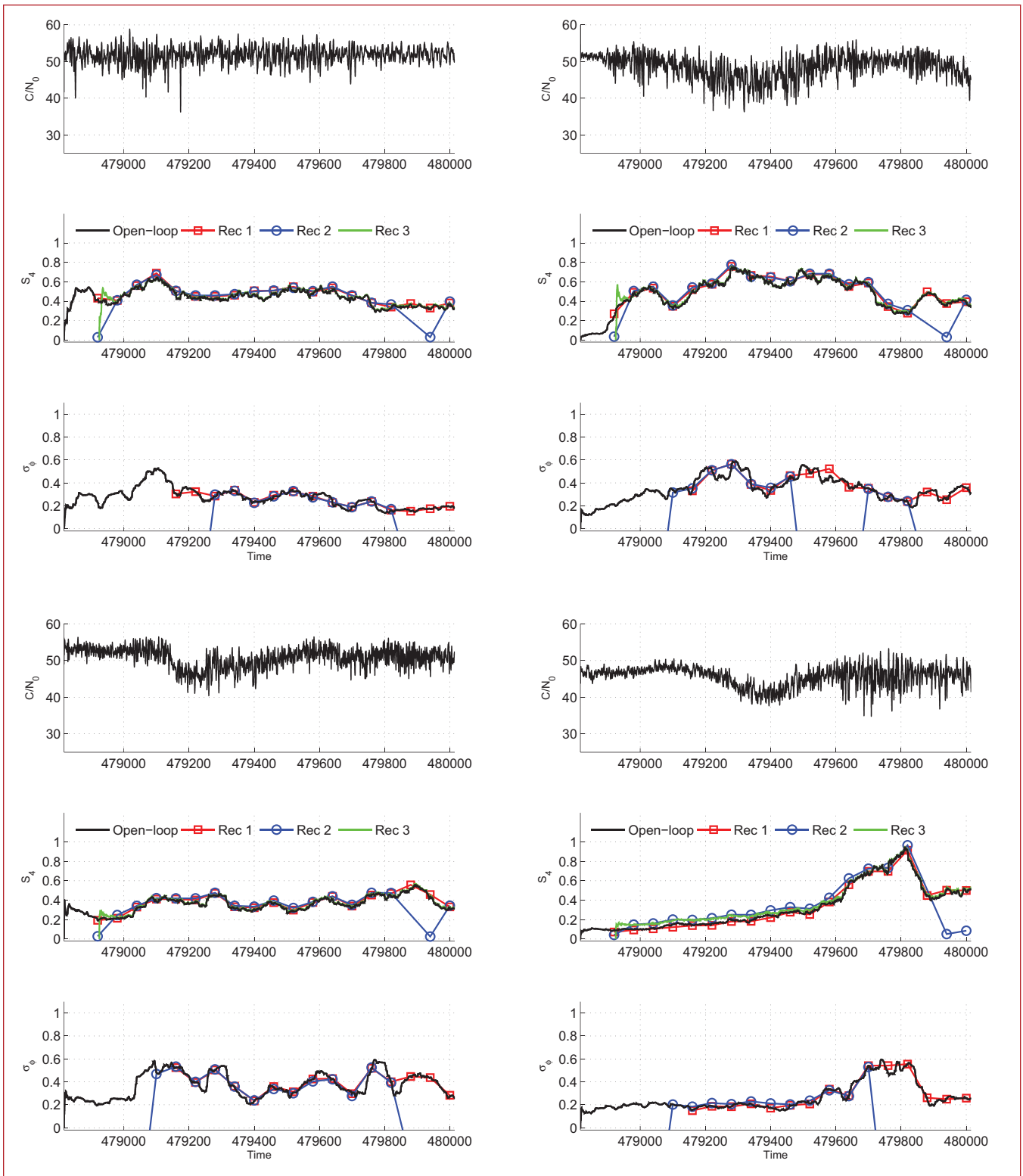


FIGURE 14 A comparison of scintillation measurements made by the new open-loop architecture and collection of commercial receivers using data collected at the Hanoi station at 13:00 UTC on the 4th of October, 2013. The loss of lock on signals is tied to zero.

(50-hertz) receiver variables, including the raw correlator values. From these values, and using equations (5) and (6), we calculated the amplitude scintillation index, S_4 .

Figure 14 presents a selection of results from a data set collected on October 4, 2013, at the Hanoi station. These preliminary results indicate that the proposed method can produce measurements that are virtually indistinguishable from those of the commercial receivers under both benign and moderate ionospheric activity. Interestingly, the open-loop scheme can sustain operation even through periods where some of the commercial receivers no longer provide measurements, most notably in the case of σ_ϕ .

JRC GNSS Scintillation Repository

The three currently operating scintillation monitoring stations record and post-process data on a daily basis. When ionospheric activity is detected, this data is archived for later use. To date more than 10 terabytes of IF data have been collected spanning 12 months, each dataset consisting of a 20 minutes of IF data, collected with 16-bit resolution at a five-megahertz complex sampling rate. Further datasets currently being gathered include four RF center frequencies, providing both Galileo and GPS multi-frequency data.

This repository of data, and data collected in the coming months will be made freely available for download by researchers. As has been shown in this article, both the resolution and the sample rate of these datasets can be significantly reduced without sacrificing measurement quality to a noticeable degree. Thus, datasets hosted will be provided at one-bit resolution and at a minimum sample rate, corresponding to a Nyquist rate that captures the signal main lobe(s), such that a large repository can be hosted and transferred with a reasonable bandwidth and mass-storage overhead.

Along with the raw IF data, reference scintillation measurements, including S_4 and σ_ϕ , computed by the architecture described here, will be provided.

The dataset are hosted on the following SFTP server: <s-jrciprvm-ftp-ext.jrc.it>. Interested parties are invited to contact the authors requesting account credentials: <james.curran@jrc.ec.europa.eu>, <michele.bavaro@jrc.ec.europa.eu>, <joaquim.fortuny@jrc.ec.europa.eu>.

Conclusions

Preliminary results from this study have demonstrated that a custom data acquisition unit coupled with an open-loop scintillation monitoring is capable of performing scintillation monitoring functions comparable to those executed by commercial solutions. The system provides a flexible, versatile platform both for data collection and archiving, and for experimentation with new scintillation monitoring algorithms. The modular and reconfigurable nature of the architecture also means that it can be scaled from single- to multi-frequency and low-cost to high-precision versions using a variety of different components.

Acknowledgments

The authors would like to thank the staff at the Jicamarca Radio Observatory (Peru Geophysics Institute) <<http://jro.igp.gob.pe>> and the NAVIS Group at the Hanoi University of Science and Technology <<http://www.hust.vn>> for their assistance and support with the installation and maintenance of the ionospheric scintillation monitoring stations.

Manufacturers

This study used a PolarRxS Ionospheric Monitoring & Space Weather receiver <<http://www.septentrio.com/products/receivers/polarxs>> from **Septentrio**, Leuven, Belgium, and the GPStation-6 GNSS Ionospheric Scintillation and TEC Monitor Receiver <<http://www.novatel.com/products/scintillation-tec-monitor/gpstation-6>> from **NovAtel, Inc.**, Calgary, Alberta, Canada. The clock-steering functionality was disabled for the NovAtel receiver, as recommended by its operating manual. Also used as a reference was the Javad Delta high-precision receiver <www.javad.com/jgnss/products/receivers/delta.html> from **Javad GNSS**, San

Jose, California, USA. A BB60C Spectrum Analyzer from **Signal Hound**, La Center, Washington, was used as part of the test configuration. The VC-OXO used in Fourtune is a refurbished Morion MV89 from **Morion, Inc.**, St. Petersburg, Russia. The SMR installation in Hanoi used a Septentrio Choke Ring MC antenna connected to a USRP-N200 front-end <<https://www.ettus.com/product/details/UN200-KIT>> from **Ettus Research**, Santa Clara, California, USA, driven by a PRS10 low phase noise rubidium clock <<http://www.thinksrs.com/products/time.htm>> from **Stanford Research Systems Inc.**, Sunnyvale, California, USA. The host PC used was a Mac-Mini from **Apple, Inc.**, Cupertino, California, USA. A PolarRxS atmospheric monitoring receiver from **Septentrio** was used to compare results. The hardware configuration used at the SINTEF campus included a permanently installed GNSS-750 choke ring antenna from **NovAtel, Inc.**

Additional Resources

- [1] Banville, S., and R. B. Langley, "Mitigating the impact of ionospheric cycle slips in GNSS observations," *Journal of Geodesy*, vol. 87, pp. 179-193, February 2013
- [2] Beach, T. L., "Perils of the GPS Phase Scintillation Index," *Radio Science*, vol. 41, October 2006
- [3] Beach, T. L., and P. M. Kintner, "Development and Use of a GPS Ionospheric Scintillation Monitor," *IEEE Transactions on Geoscience and Remote Sensing*, vol. 39, no. 5, pp. 918- 928, 2001
- [4] Fremouw, E. J., and R. L. Leadabrand, R. C. Livingston, M. Cousins, C. L. Rino, B. Fair, and R. A. Long, "Early Results from the DNA Wideband Satellite Experiment - Complex-signal Scintillation," *Radio Science*, vol. 13, pp. »167-187«, 1978
- [5] Humphreys, T., and M. Psiaki, J. Hinks, B. O'Hanlon, and P. Kintner, "Simulating Ionosphere-Induced Scintillation for Testing GPS Receiver Phase Tracking Loops," *IEEE Journal of Selected Topics in Signal Processing*, vol. 3, no. 4, pp. 707-715, 2009
- [6] Van Dierendonck, A. J., J. Klobuchar, and Q. Hua, "Ionospheric scintillation monitoring Using Commercial Single Frequency C/A Code Receivers," *Proceedings of the 6th International Technical Meeting of the Satellite Division of*

The Institute of Navigation (ION GPS 1993), pp. 1333–1342, September 1993

[7] Yeh, K. C., and C.-H. Liu, "Radio Wave Scintillations in the Ionosphere," *Proceedings of the IEEE*, vol. 70, no. 4, pp. 324–360, 1982

Authors



James T. Curran received a B.E. in electrical & electronic Engineering and a Ph.D. in telecommunications from the Department of Electrical Engineering, University College Cork, Ireland. He worked as a senior research engineer with the PLAN Group in the University of Calgary from 2011 and is currently a grant-holder at the Joint Research Center (JRC) of the European Commission (EC), Italy. His main research interests are signal processing, information theory, cryptography, and software defined radio for GNSS.

Michele Bavaro received his master degree in computer science from the University of Pisa, Italy. Shortly afterwards he started his work on software defined radio technologies applied to navigation. First in Italy, then in The Netherlands and in the UK he worked on several projects being directly



involved with the design, manufacture, integration, and test of radionavigation satellite system (RDSS) equipment and supporting customers in the development of their applications.

Today he is appointed as grant-holder at the EC JRC.



Aiden Morrison received a B. Eng. in Electrical Engineering and a Ph.D. in Geomatics from the University of Calgary. He has since worked as a designer of RF and navigation systems at the University of Calgary, Norbit group, and is currently employed at the SINTEF research institute in Trondheim, Norway.



Joaquim Fortuny-Guasch received the engineering degree in telecommunications from the Technical University of Catalonia (UPC), Barcelona, Spain and the Dr.-Ing. degree in electrical engineering from the Universitat Karl-

sruhe (TH), Karlsruhe, Germany. Since 1993, he has been working for the Joint Research Centre of the European Commission, Ispra, Italy, as senior scientific officer. He is the head of the European Microwave Signature Laboratory and leads the JRC research group on GNSS and wireless communications systems.



Prof.-Dr. Günter Hein serves as the editor of the Working Papers column. He is the head of the EGNOS and GNSS Evolution Program Department of the European Space Agency. Previously, he was a full professor and director of the Institute of Geodesy and Navigation at the Universität der Bundeswehr München. In 2002, he received the Johannes Kepler Award from the U.S. Institute of Navigation (ION) for "sustained and significant contributions" to satellite navigation. He is one of the inventors of the CBOC signal. 



THE INSTITUTE OF NAVIGATION
2015 International Technical Meeting

Laguna Cliffs Marriott Hotel, Dana Point, California

January 26-28, 2015

Plenary Session

The Human Factor: Interpreting and Acting on Navigation Data

- Advanced RAIM and Autonomous Integrity
- Alternative Sensors and Emerging Navigation Technologies
- Augmentation Systems (SBAS and GBAS)
- Aviation and Marine Applications
- Collaborative Sensing and Multisensor Fusion
- Emerging GNSS and Modernization
- GNSS Processing and Integration
- Human-Centered Navigation
- Interference, Spectrum Management, and Backups to GNSS
- MEMS, Timing and Micro PNT
- Quasi-Zenith Satellite System
- Receivers and Antenna Technology
- Robot and Autonomous Vehicle Navigation
- Space and Atmospheric Weather
- Urban, Indoor and Terrestrial Applications

Register Today! www.ion.org/itm

